



# Influence of Nb on the Hot Corrosion Behaviors of a Fe–Cr–Ni Heat-Resistant Steel Weld Metal in the Na<sub>2</sub>SO<sub>4</sub>–NaCl Molten Salt at 700 °C

Zhang Xu<sup>1,3</sup> · Wan Jinchu<sup>1</sup> · Zhu liang<sup>1</sup> · Zhou Hui<sup>2</sup> · Yang Zonghui<sup>1,3</sup>

Received: 9 February 2023 / Accepted: 8 May 2023 / Published online: 2 June 2023  
© The Author(s) under exclusive licence to The Korean Institute of Metals and Materials 2023

## Abstract

A multiple gas tungsten arc welding was performed on the fabrication of the Fe–Cr–Ni-based weld metal. Microstructures and hot corrosion behaviors of the non-equilibrium weld metals with different Nb contents in 75 wt%Na<sub>2</sub>SO<sub>4</sub>–25 wt%NaCl molten salt at 700 °C have been investigated. A bilayer oxide film composed of an inner Cr<sub>2</sub>O<sub>3</sub> layer and an outer Fe<sub>2</sub>O<sub>3</sub> layer formed on the surface of the weld metals. The mass gain rate and the thickness of the surface oxide film were enlarged with Nb addition, which could be attributed to the rapid inward diffusion of O through the cracks resulting from the Nb-oxide. Oxidation and sulfidation occur in the matrix, resulting in a large internal oxidation zone (IOZ) in the weld metal. Nb seemingly promoted the sulfidation reaction due to a short-circuit diffusion of S through the interface of the Nb(C, N) and matrix and made the internal corrosion products to be distributed along the interdendritic zone of the weld metal. An apparent Cr-dealloyed layer appears in the IOZ of the weld metal. Dealloying was the detrimental form of hot corrosion of Fe–Cr–Ni-based weld metal exposed to molten salts containing chloride salts. Alloying with 0.8 wt% of Nb further accelerated the dealloying and resulted in a profound attack.

**Keywords** Fe–Cr–Ni weld metal · GTAW · Hot corrosion · Nb · Oxide scale · Diffusion

## 1 Introduction

Welding technology is generally an important process in the fabrication of key components in the fields of nuclear power plants or thermal power plants, like steam generation tubes and superheaters [1, 2]. Austenitic heat-resistant steel welding material has been widely applied to the above fields due to its comprehensive mechanical properties, excellent oxidation resistance and low price [3]. Generally, weld metals will face considerable challenges in elevated temperature harsh environments as same as the base materials. Due to

coarse solidification microstructure and welding defects, weld metals usually have poor high-temperature performances in actual service and are considered weak points for the components. The properties of the weld joints are just regarded as the key point to directly determine the service life of the components. Numerous outstanding jobs have been performed to study the relationship between the microstructures and properties of weld metals, and then provide many methods to improve the high-temperature performance of the weld metals [4, 5]. Microalloying, welding process parameters and heat treatments are common useful methods to control the microstructure and properties of weld metals [6–8].

Niobium is an important microalloying element to improve the mechanical properties of metals and alloys [9, 10]. The strength of alloys would be enhanced by solid solution strengthening and precipitation strengthening resulting from the element Nb. However, alloys could be damaged at elevated temperatures by a process called hot corrosion [11]. In most high-temperature environments, the thin oxide film formed on the surface of Fe- and Ni-based alloys protects them from corrosion. However, the oxide layer breaks

✉ Zhang Xu  
zhangxu@njit.edu.cn

<sup>1</sup> School of Materials Science and Engineering, Nanjing Institute of Technology, Nanjing 211167, China

<sup>2</sup> School of Materials Science and Engineering, Lanzhou University of Technology, Lanzhou 730050, China

<sup>3</sup> Jiangsu Key Laboratory of Advanced Structural Materials and Application Technology, Nanjing Institute of Technology, Nanjing 211167, China

down and alloys undergo selective dissolution (dealloying) of reactive elements (e.g. Fe, Cr, Mn) in high-temperature molten salt environments [12]. Generally, hot corrosion is not expected in pure molten salts but it is the fact that chloride salts contain moisture, which is hard to be completely removed, and upon melting residual moisture content reacts with chloride ions and forms highly soluble HCl that is highly corrosive. Morphology of dealloyed layer later upon dealloying of Cr and Fe from Ni-based alloys exposed to molten halide salts depends on the atom fraction of Ni in the alloy and the operating temperature, involves the formation of Ni enriched layer with subsurface void and/or porous structure rich in Ni associated with perforating nature of dealloyed layer and molten salts [13–15]. Therefore, the hot corrosion resistance of structural materials including weld materials in the molten salt environment is as important as the mechanical properties, affecting the service life of the components directly. A stable and dense surface oxide film is the key to affecting the hot corrosion resistance of alloys. It is reported that chlorides and sulfates are the two main salts that lead to the hot corrosion failure of alloys [16, 17]. Oxygen-containing molten salts do not promote dealloying. However, dealloying occurs in molten chloride salts. Therefore, many works have focused on the hot corrosion behaviors of heat-resistant alloys in molten chlorides and/or sulfates at elevated temperatures and the failures of the surface oxide film have been investigated.

Nowadays, the role of niobium in the hot corrosion behavior of alloys in molten salts has been reported. Zhou et al. [18] investigated the hot corrosion behaviors of two Ni-based superalloys with and without minor Nb under molten  $\text{Na}_2\text{SO}_4$  at 900 °C. They indicated that minor Nb could accelerate the formation of chromia scale and inhibit the internal oxidation/nitridation, leading to a lower scaling rate. Xu et al. [19] added 1 wt% Nb to Ni–Cr alloy and found that Nb improved Cr activity and NbC particles precipitating along grain boundaries suppress the outward diffusion of Fe and Ni. Nb has a beneficial effect on the oxidation resistance of Ni–Cr alloy. However, Dai et al. [20] added Nb into TiAl coating and reported that adding too much Nb to the coating deteriorated the hot corrosion resistance of the coating. Jia et al. [21] also reported that the formation of the Laves phase was promoted by Nb addition, which increased the oxidation parabolic rate constant. The difference in previous research results could be attributed to the Nb content and the Nb-forming precipitates, like carbides, Laves phase,

and G phase. The corrosion resistance and thermal stability of those precipitates are different, which will result in complex element diffusion behaviors and dealloying in alloys at elevated temperatures [22].

Due to the unique welding heat input, weld metals are non-equilibrium solidification microstructures [23]. The distribution of composition and second particles has a significant difference with base materials. Nb is a negative segregation element. Wu et al. [24] investigated the solidification of the Ni–Fe-based weld metal and reported that Nb tends to segregate to interdendritic regions during the solidification process. Nb-forming precipitates generally form along the columnar dendrite and were distributed in a chain. The unique distribution of Nb elements and precipitates may result in the special hot corrosion behavior of weld metals. Therefore, the influence of Nb on the hot corrosion behaviors of weld metals needs to be given more attention.

In the present research, element Nb was added to the Fe–Cr–Ni-based austenitic heat-resistant steel weld metal and its effect on the microstructure and hot corrosion behaviors of the weld metals was investigated. OM and SEM were performed to observe the microstructure and surface corrosion morphologies of weld metals with different Nb addition. The composition distribution and structures of hot corrosion products were analyzed by EDS and XRD, respectively.

## 2 Materials and Preparations

### 2.1 Materials and Welding

A 310 s austenitic heat-resistant steel and two welding wires with different Nb contents, labeled as 0Nb and 0.8Nb, were prepared as base material and filler metals, respectively. The chemical compositions of the above experimental materials are given in Table 1. The base material is 300 mm × 100 mm × 16 mm in dimension and the diameter of the welding wires is about  $\Phi 1.2$  mm. A multiple gas tungsten arc welding (GTAW) was then employed in the butt welding experiment and the corresponding schematic diagram of the butt joint is shown in Fig. 1. The angle of the butting groove in the present research is about 60°. The specific welding parameters are given in Table 2. After welding, all weld metals were detected by an X-ray inspection to discover whether there were any welding defects existing

**Table 1** Chemical composition of the base material and welding wires (wt%)

	C	Cr	Ni	Si	Mn	N	Nb	Fe
310S	0.055	25.10	19.71	0.49	0.97	–	–	Bal.
0Nb	0.084	25.89	20.90	0.51	1.65	0.10	–	Bal.
0.8Nb	0.092	26.14	21.02	0.48	1.70	0.098	0.78	Bal.

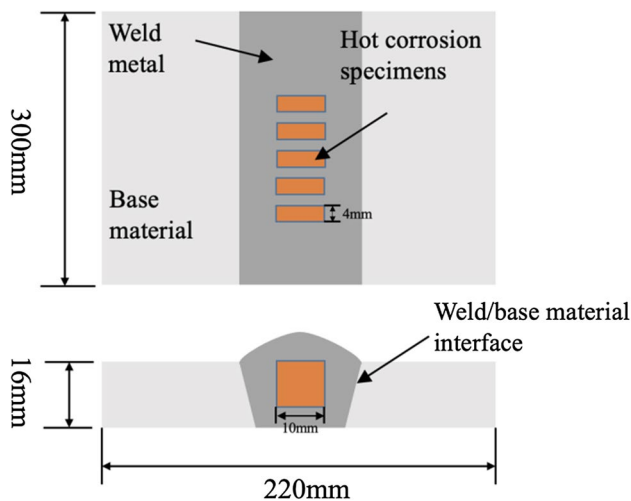


**Fig. 1** Schematic diagram of the weld joint and the sampling location of the hot corrosion specimens

in the interior of the weldments. The experimental samples should be cut from the part without any welding defects to ensure the reliability of the hot corrosion test.

## 2.2 Hot Corrosion Test

The hot corrosion test samples with a dimension of 10 mm × 10 mm × 4 mm were cut with a wire electrical discharge machining (WEDM) from the core of weld metals and away from the interface of weld metal and base material, which would avoid the influence of the chemical composition dilution on the hot corrosion behavior of weld metal, as shown in Fig. 1. The specimens were then ground with 150, 240, 400, 800, 1200 and 2000 grid sandpapers and cleaned ultrasonically in alcohol prior to hot corrosion tests. A drying oven was performed to keep specimens at 50 °C for 10 h after cleaning, which helps to achieve accurate weights of the original weld metals without the influence of residual alcohol. Laboratory-grade Na<sub>2</sub>SO<sub>4</sub> and NaCl, purchased from China National Pharmaceutical Group Co., Ltd., were dissolved in deionized water at a weight ratio of 3:1 to prepare a saturated solution. The coupons were heated on a hot plate to approximately 200 °C while simultaneously applying the salt mixture to the surface by spraying the saturated solution with a spray gun. The test coupons were weighed regularly to ensure that the proper quantity of mixed salt was deposited on surfaces during the salt application. Approximately 5.0 ± 0.2 mg/cm<sup>2</sup> of the salt mixture was controlled

to be deposited on each specimen. Samples were then kept at 700 °C for 5 h, 10 h, 20 h, 30 h, 50 h, 70 h and 100 h in ambient air in a muffle furnace for the hot corrosion test. To get rid of the influence of the spallation of surface oxide scales on the weight gain measurement during hot corrosion test or cooling, samples would be put into corundum crucibles sealed with a cover. Three parallel specimens were prepared for each duration to ensure the reliability of the experiments. The weight gain changes of the specimens were measured by an analytical balance with an accuracy of 0.01 mg in each duration.

## 2.3 Microstructure Characterization

Samples were prepared with a traditional mechanical grinding and polishing process and then etched at 10 V in a 10% oxalic acid reagent for microstructure observation. The microstructures of the as-welded alloys with different Nb addition as well as the surface morphologies of the oxide scales on hot corrosion test samples were observed by a Merlin Compact field emission SEM. The samples were cleaned after hot molten salt corrosion experiments and the crystallographic structures of the surface oxide scales of the investigated weld metals at various hot corrosion durations were characterized by a Bruker D2 Phaser XRD with Cu K $\alpha$  radiation at 30 kV in the 2 $\theta$  range of 10–90° with the scanning step of 2°/min. Hot corroded samples were cut into two parts from the middle with WEDM. The cross-section of the oxide scales of one part was mounted with epoxy resin and also prepared with a traditional grinding and polishing process for microstructure observation. The element distributions in weld metals as well as the compositions of the precipitates in the matrix were analyzed by an EDS equipped on an SEM.

## 3 Results and Discussions

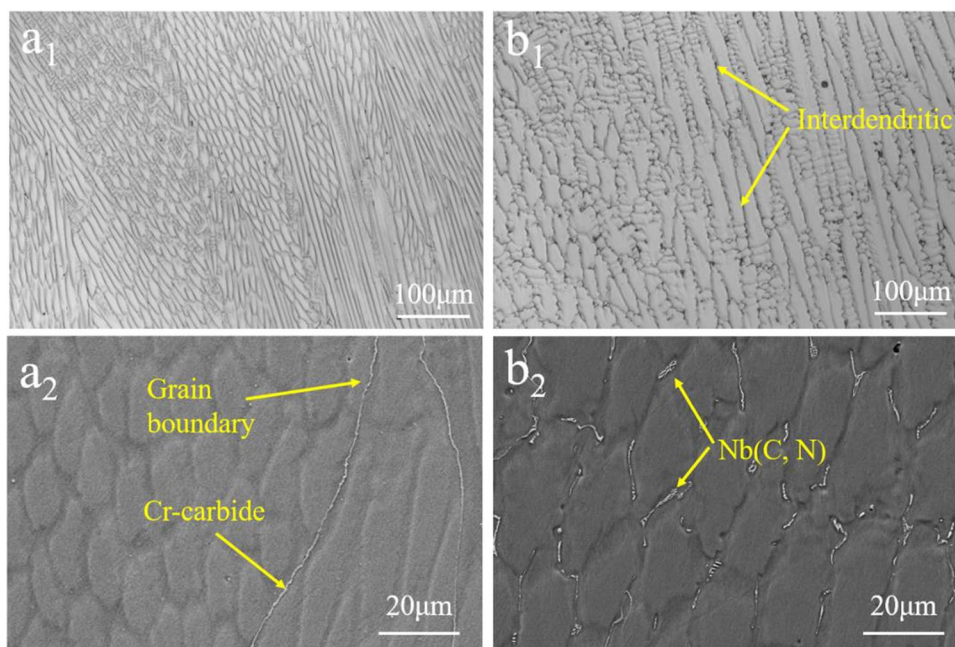
### 3.1 Microstructures of Fe–Cr–Ni-Based Weld Metals with Different Nb Contents

Microstructures of the weld metals with different Nb contents observed by OM and SEM are given in Fig. 2. The large columnar dendrites indicated a typical as-welded metal microstructure. With the Nb addition, the secondary dendrite arm space is enlarged, as shown in Fig. 2(a<sub>1</sub>, b<sub>1</sub>). Due to the high Cr content, there are amounts of Cr-carbides

**Table 2** Welding parameters

Current (A)	Voltage (V)	Wire feed speed (mm/min)	Travel speed (mm/min)	Gas flow rate (L/min)	shielding gas	Interpass temperature(°C)
180	12	1100	110	15	99.999% Ar	< 150

**Fig. 2** OM and SEM images for microstructures of the Fe–Cr–Ni-based weld metals with different Nb contents: (**a**<sub>1</sub>, **a**<sub>2</sub>) 0Nb, (**b**<sub>1</sub>, **b**<sub>2</sub>) 0.8Nb



precipitating along the grain boundaries in the 0Nb weld metal. However, no secondary particles could be found in the core of dendrites or interdendritic regions. Elemental Nb has a strong affinity with elemental C and could promote the formation of NbC carbide at high temperatures [25]. With 0.8 wt% Nb addition, Nb(C, N) would precipitate in the weld metal, as shown in Fig. 2(b<sub>2</sub>). Due to the high cooling rate, the diffusion of elements is generally insufficient and element segregation is a common phenomenon in weld metals during the welding process [26]. Typically, Nb is a negative segregation element and it just tends to segregate in the liquid during the solidification. Thus the interdendritic zones will be rich in Nb and the core of dendrites will be poor in Nb. Second particles Nb(C, N) just are distributed in a chain in the interdendritic zone.

### 3.2 Effect of Nb on the Hot Corrosion Behaviors of the Fe–Cr–Ni-Based Weld Metal

Figure 3 gives the mass changes of weld metals with or without Nb after being exposed to 700 °C in the Na<sub>2</sub>SO<sub>4</sub>–NaCl molten salts. The result shows that the weight gains of weld metals with different Nb contents follow a parabolic law, indicating a diffusion control process at high temperatures. The corresponding parabolic rate constants [27], which reflect the hot corrosion rate of alloy, are calculated based on polt curves in Fig. 3. The values of the parabolic rate constants for 0Nb and 0.8Nb weld metals are  $1.35 \times 10^{-9} \text{ g}^2 \cdot \text{cm}^{-4} / \text{s}$  and  $2.76 \times 10^{-9} \text{ g}^2 \cdot \text{cm}^{-4} / \text{s}$ , respectively. It is obvious that the weld metal with the elemental Nb addition exhibits a higher weight gain at each time in comparison to the Nb-free weld metal. That is, elemental Nb

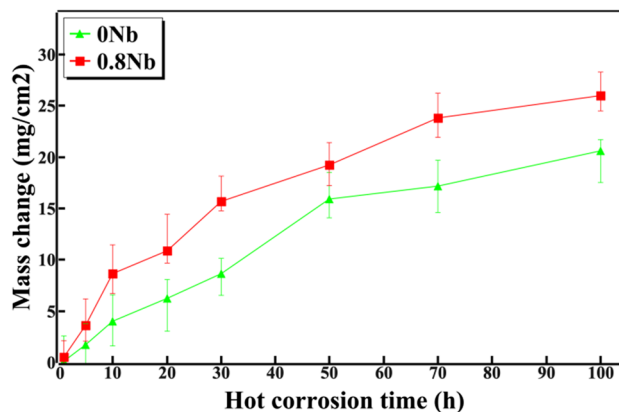


**Fig. 3** Mass change vs. hot corrosion time for weld metals with different Nb contents after being exposed to 700 °C in the 75 wt% Na<sub>2</sub>SO<sub>4</sub>–25 wt%NaCl mixed molten salts

accelerates the hot corrosion of Fe–Cr–Ni-based heat-resistance steel weld metal and is harmful to the high-temperature performances of weld metals.

Many hot corrosion products could be generated on the surface of weld metals at elevated temperatures with 75 wt%Na<sub>2</sub>SO<sub>4</sub>–25 wt%NaCl mixed molten salts. Figure 4 gives the XRD patterns of the weld metals containing different Nb contents after hot corrosion at 700 °C for 100 h. According to the results of the XRD patterns, the surface corrosion products for 0Nb and 0.8Nb weld metals have no apparent differences and are mainly composed of Cr<sub>2</sub>O<sub>3</sub>, Fe<sub>2</sub>O<sub>3</sub> and Fe + 2Cr<sub>2</sub>O<sub>4</sub>. Fe + 2Cr<sub>2</sub>O<sub>4</sub> is generally a mixture structure consisting of Cr<sub>2</sub>O<sub>3</sub> and Fe<sub>2</sub>O<sub>3</sub>, which has been reported in previous literature [28]. Depending on the



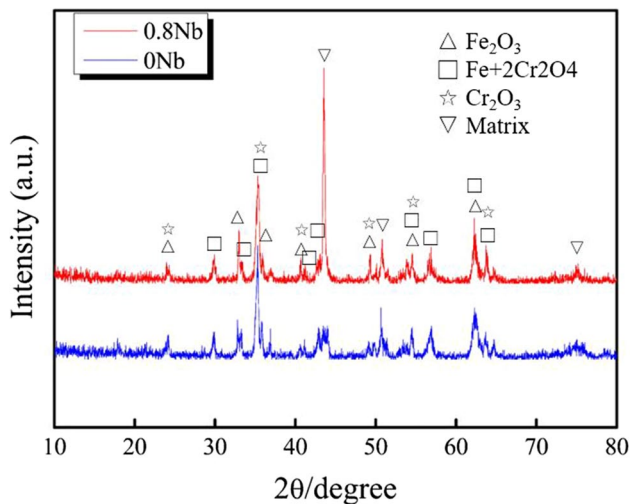


**Fig.4** XRD patterns of the weld metals with different Nb contents after being exposed to molten  $\text{Na}_2\text{SO}_4$ – $\text{NaCl}$  salt mixture at  $700\text{ }^\circ\text{C}$  for 100 h

diffraction peak relative intensity, it is seemly that the corrosion products on the 0.8Nb weld metal are more than those on the 0Nb weld metal. That is, oxygen could diffuse easily into the matrix to form more oxides when the element Nb is added to weld metal.

Figure 5 gives surface morphologies of the oxide scales formed on the weld metals with different Nb contents after

being exposed to  $\text{Na}_2\text{SO}_4$ – $\text{NaCl}$  salts mixture at  $700\text{ }^\circ\text{C}$  for 100 h. It is easy to note that heavy spallation occurred in both two investigated weld metals, which may be caused by the oxides generation stress or the thermal stress. Based on the morphologies of the spallation zone, the fact that the oxide films formed on the surface of the weld metals have a multilayer structure is easy to find. The inner oxide layer is relatively flat and dense. However, the outer oxide layer is uneven and loose, as shown in Fig. 5( $a_1$ ,  $a_2$ ,  $b_1$ ,  $b_2$ ). Meanwhile, there are amounts of oxide nodules appearing on the outer oxide layer. The phenomenon can be attributed to the different diffusion rates of the element on the surface of the weld metal during the hot corrosion process, which was also reported by other researchers [29]. With Nb addition, the size of oxide nodules becomes large, indicating that Nb promotes the chemical reaction on the surface of weld metals due to enlarged element segregation. The EDS results indicated that the inner oxide layer is rich in element Cr and the outer oxide layer is rich in element Fe. Combined with the analysis result by XRD in Fig. 4, it is easy to infer that the inner oxide and the outer oxide may be  $\text{Cr}_2\text{O}_3$  and  $\text{Fe}_2\text{O}_3$ , respectively.

Figure 6 shows cross-section morphologies of the oxide scales on the Fe–Cr–Ni-based weld metals with different Nb contents, which were exposed to  $\text{Na}_2\text{SO}_4$ – $\text{NaCl}$  mixed molten salts at  $700\text{ }^\circ\text{C}$  up to 100 h. A bilayer oxide scale composed of the inner layer of  $\text{Cr}_2\text{O}_3$  and the outer layer of  $\text{Fe}_2\text{O}_3$  appeared on the surfaces of the weld metals, which

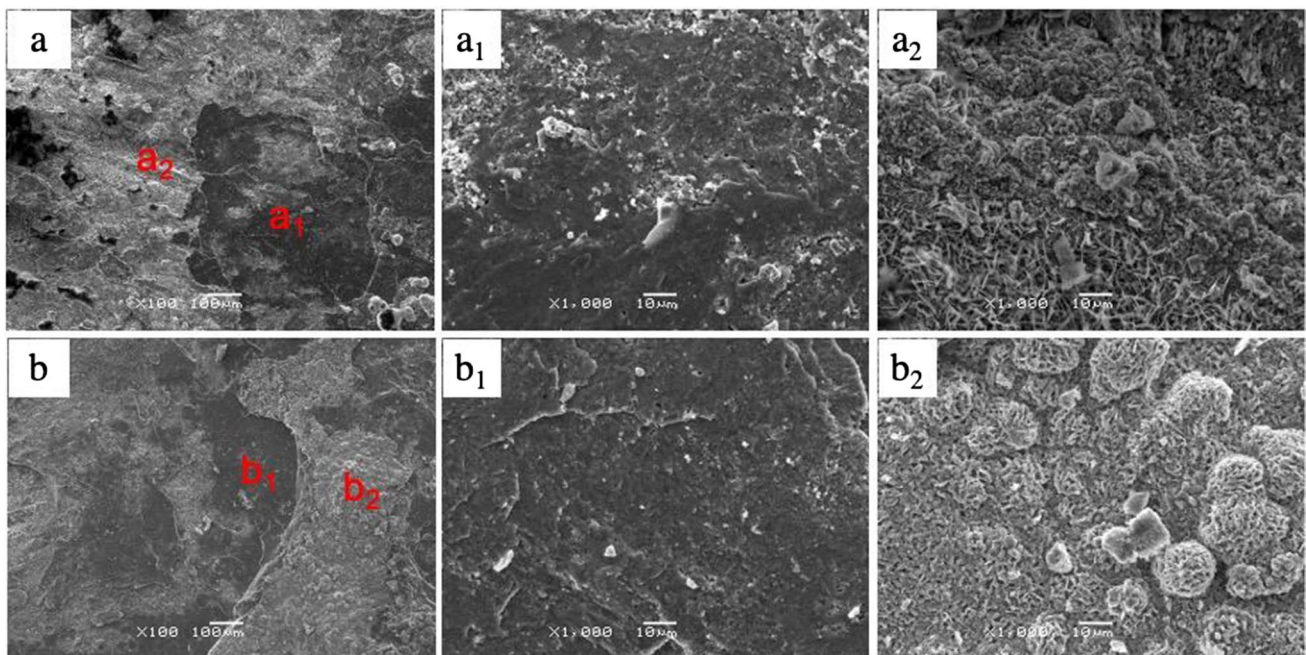
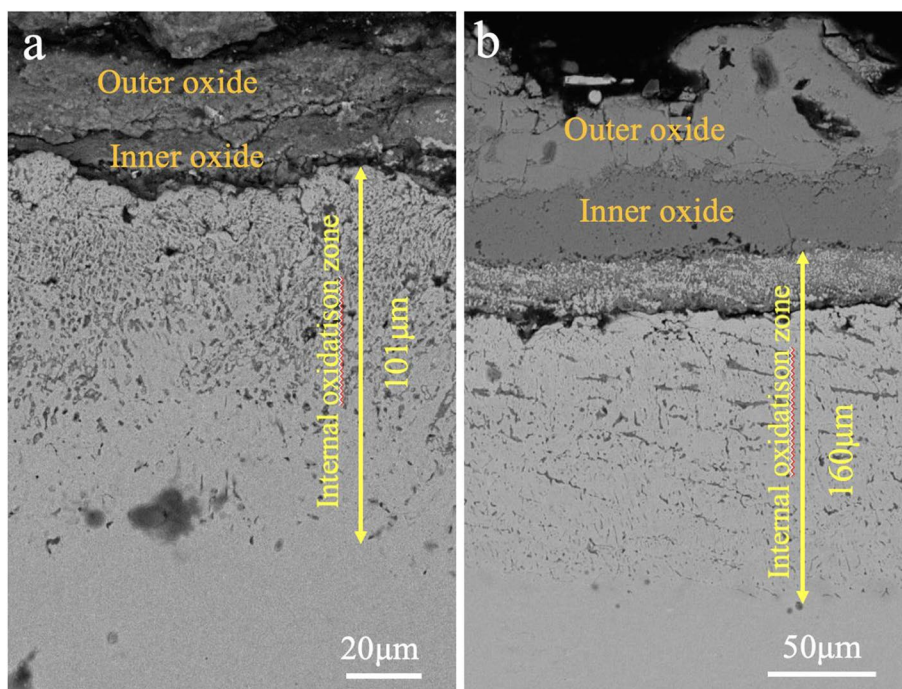


**Fig.5** Surface morphologies of the oxide films on the weld metals with different Nb contents after being exposed to molten  $\text{Na}_2\text{SO}_4$ – $\text{NaCl}$  salt mixture at  $700\text{ }^\circ\text{C}$  for 100 h: (**a**, **a**<sub>1</sub>, **a**<sub>2</sub>) 0Nb, (**b**, **b**<sub>1</sub>, **b**<sub>2</sub>)

0.8Nb; (**a**<sub>1</sub>, **a**<sub>2</sub>) were magnification images for the part labeled as **a**<sub>1</sub> and **a**<sub>2</sub> in the image **a**, respectively; (**b**<sub>1</sub>, **b**<sub>2</sub>) were magnification images for the part labeled as **b**<sub>1</sub> and **b**<sub>2</sub> in the image **b**, respectively

**Fig. 6** SEM observation for cross-section morphologies of the surface oxide scales on the weld metals containing different Nb contents after being exposed to molten  $\text{Na}_2\text{SO}_4$ – $\text{NaCl}$  salt mixture at 700 °C for 100 h: **a** 0Nb, **b** 0.8Nb



was consistent with the results of the surface morphologies observation in Fig. 5. The average thicknesses of the bilayer oxide scales for the Nb-free and Nb-bearing weld metal are about 35  $\mu\text{m}$  and 78  $\mu\text{m}$ , respectively. Further, the oxide film is not dense and can not hinder inward and outward diffusions of anions and cations. Pores and crackings are easy to be observed in the bilayer oxide film of the Nb-bearing weld metal after being hot corroded in the molten salts for 100 h, as shown in Fig. 6b. In addition, a large internal oxidation zone (IOZ) appears under surface oxide scales, showing an apparent dealloyed layer. The dealloyed region is associated with the penetration of molten salts to the metal lattice where corrosion in the form of dealloying has proceeded in the bulk solid. The dealloying phenomenon is further discussed in the subsequent section. The width of the IOZ in the weld metal 0Nb and 0.8Nb is 101  $\mu\text{m}$  and 160  $\mu\text{m}$ , respectively. Nb addition correspondingly enlarged the width of the IOZ of the Fe–Cr–Ni-based weld metal. Noteworthy, the morphologies of the IOZ present significant differences in the two weld metals, indicating that the ions' diffusion behaviors in the matrix could be affected by the element Nb. The distribution of the oxide in the 0Nb weld metal is relatively uniform from the oxide scale/metal interface to the core of the matrix. Although some internal oxides in the IOZ of the 0.8Nb weld metal are distributed evenly as same as that in the 0Nb weld metal, large oxides distributing in stripes were also found clearly, as shown in Fig. 6b. Based on the observation of the microstructure of the as-welded metal, it is easy to deduce that the large oxides just formed along the interdendritic zone. Further, the large

oxide in stripes just occupied the original Nb-carbide in the interdendritic zone and then grow into the matrix, as shown in Fig. 7. The phenomenon seemingly indicated that the Nb-carbide promoted the short-circuit diffusion of the oxygen at high temperature, which accounts for the fact that the width of the IOZ become larger with Nb addition.

EDS scanning was performed on the 0Nb and 0.8Nb weld metals after hot corrosion in the molten salts for 100 h and the corresponding results are given in Fig. 8. An apparent Cr depletion zone appears under the bilayer oxide film. As

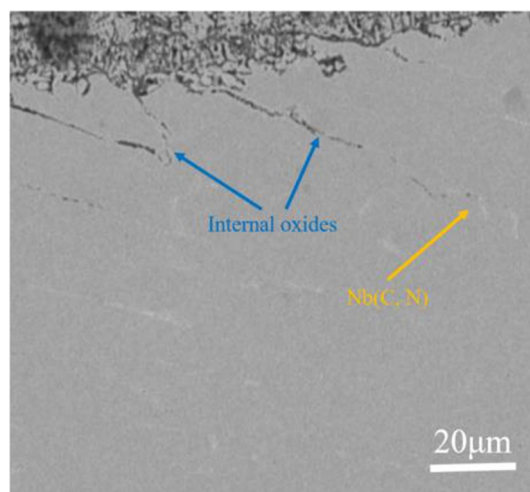


**Fig. 7** The relationship between internal oxides and Nb-carbide in the Nb-bearing weld metal after being exposed to molten  $\text{Na}_2\text{SO}_4$ – $\text{NaCl}$  salt mixture at 700 °C for 100 h



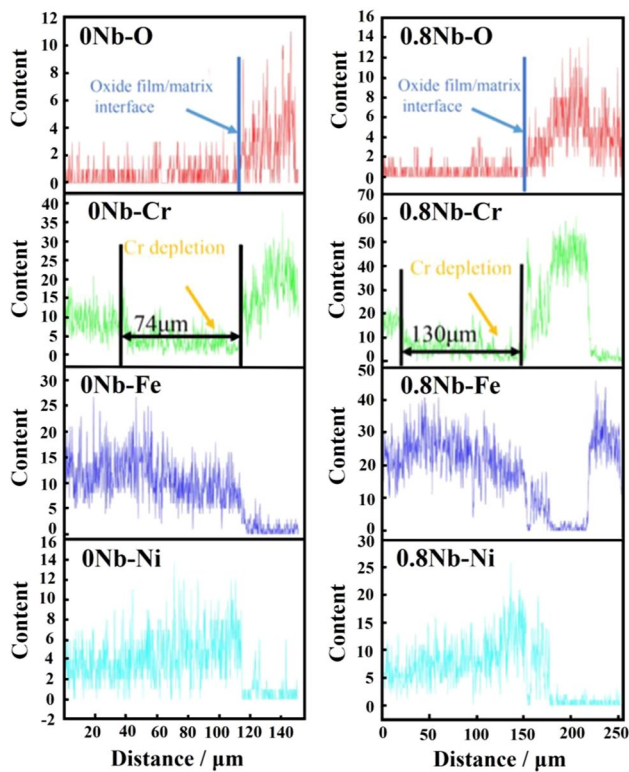


**Fig. 8** EDS line scan for the internal oxidation zone, oxide scales, and dealloyed layer formed on the weld metals with and without Nb after molten salt corrosion experiment at 700 °C for 100 h

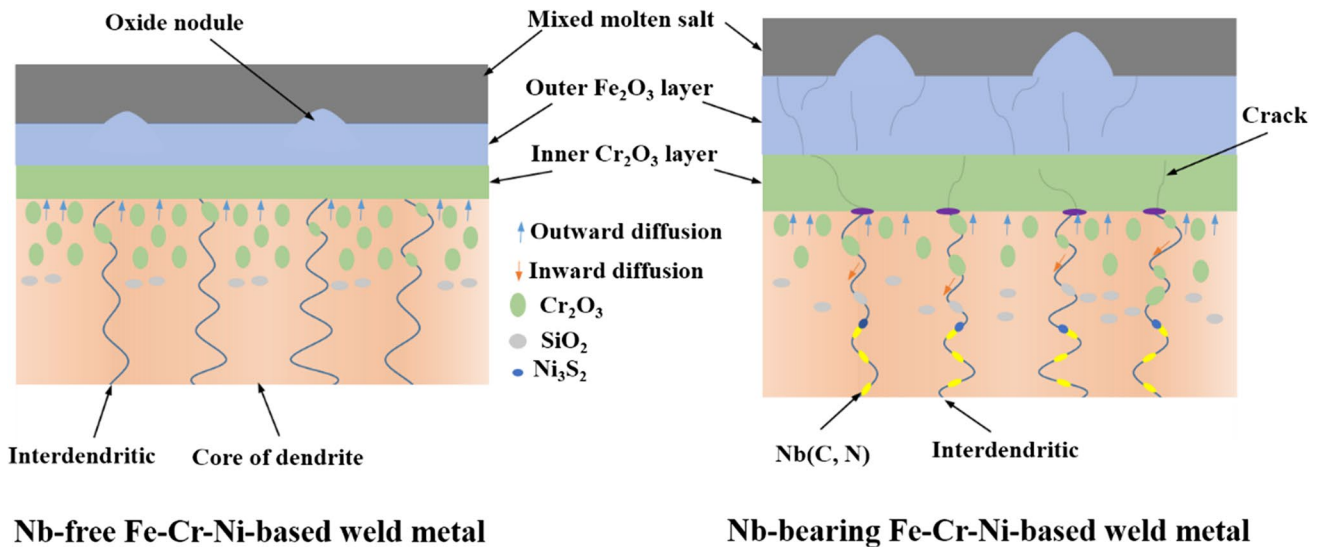
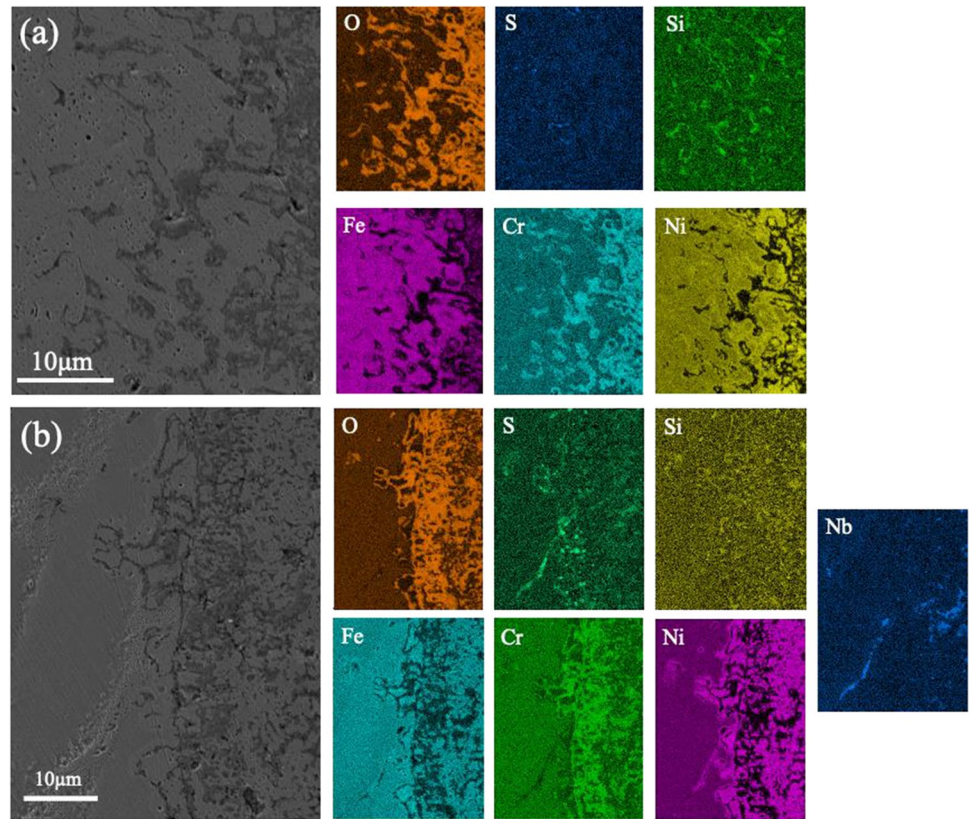
discussed in the Introduction, dealloying is one detrimental mode of corrosion in molten chloride salts where reactive elements selectively dissolve out of alloys. Similarly, our study also confirmed that dealloying of Cr and enrichment of Ni occur for weld metals exposed to molten salts containing 25 wt%NaCl as seen in Fig. 8, which highlights the detrimental effect of Cl salts. The width of the Cr depletion zone for Nb-free and Nb-bearing weld metal is about 74  $\mu\text{m}$  and 130  $\mu\text{m}$ , respectively. The depth of attack and associated Cr-depleted layer further increased for Fe–Cr–Ni weld metal containing minor content of Nb, which suggests the detrimental effect of Nb for the molten salt system. At high temperatures, Cr in the matrix would outward diffuse to react with the oxygen at the molten salt/weld metal interface and then promotes the protective  $\text{Cr}_2\text{O}_3$  oxide scale form on the surface of weld metal. The surface oxide cluster is not protective and molten salt containing remnant impurities such as oxygen and moisture penetrate into bulk weld metal as dealloying proceeds, where oxygen and moisture further oxidized Cr from underlying sites that subsequently dissolve away and corrosion proceeds. Due to the selective dissolution of Cr and the lack of sufficient replenishment of internal element Cr, Cr depletion would occur under the surface of weld metals.

Figure 9 gives the element mapping distribution of IOZ for the weld metals with different Nb additions after exposure to 700 °C for 100 h. The results indicate that the internal products are Cr-oxide ( $\text{Cr}_2\text{O}_3$ ) and Si-oxide ( $\text{SiO}_2$ ). In present Fe–Cr–Ni-based weld metal, Si content (about 0.5 wt%) is much lower than Cr content (about 26 wt%). Although Si has a higher affinity for O at high temperatures than Cr based on the Ellingham diagram, Cr-oxides are still the main internal oxidation products, as shown in Fig. 9a. Moreover, S is distributed at the interface of the IOZ and matrix and is not nearly found elsewhere. That is, sulfidation occurs at the front of the IOZ in the present weld metal during the hot corrosion process. Compared to Nb-free weld metal, the Nb-bearing weld metal seemly suffer severer sulfidation, as shown in Fig. 9b. It is worth noting that the distribution of elements S, Nb and Ni is partially consistent. According to the microstructures of Nb-bearing weld metal, Nb(C, N) is the primary phase and is distributed along the interdendritic zone in the weld metal. Nb(C, N) particles may provide a fast-channel diffusion for element S.

Based on the above results, A brief and clear schematic diagram for the hot corrosion mechanism of the weld metals with different Nb contents in  $\text{Na}_2\text{SO}_4$ –NaCl molten salt was given in Fig. 10. The hot corrosion mechanism of the Fe–Cr–Ni-based weld metal in  $\text{Na}_2\text{SO}_4$ –NaCl molten salt at 700 °C and the role of element Nb could be discussed as follows:

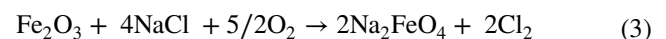
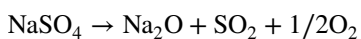
$\text{Cr}_2\text{O}_3$  forms on the Fe–Cr–Ni-based weld metal at elevated temperatures due to the preferential combination of Cr and O in the molten salt/metal interface [30]. Previous research has reported that the Cr content for maintaining continuous dense  $\text{Cr}_2\text{O}_3$  oxide film on the surface of alloys is at least 12 wt% [31]. The high Cr content (about 26 wt%) of investigated weld metal is enough to promote the formation of the continuous  $\text{Cr}_2\text{O}_3$  oxide layer (Fig. 5). Elemental Fe diffuses through the dense  $\text{Cr}_2\text{O}_3$  layer and reacts with oxygen to form  $\text{Fe}_2\text{O}_3$  above the surface of  $\text{Cr}_2\text{O}_3$ . Hence, a bilayer oxide scale composed of the inner chromia layer and the outer  $\text{Fe}_2\text{O}_3$  layer appears on the surface of the weld metals. Noteworthy, chemical segregation is a common phenomenon in the weld metal, the content of Cr, Fe and Ni in the core of dendrites and the interdendritic zone is different, which results in a difference in the outward diffusion of ions. Hence, oxide nodules appeared on the surfaces of the oxide layer (Fig. 5). Generally, the bilayer oxide scale could hinder the repaid inward diffusion of O and protect the weld metals from continuous oxidation at high temperatures. However, the oxide scale will break down for a molten salt mixture that contains chloride salts. The 75 wt% $\text{Na}_2\text{SO}_4$ –25 wt%NaCl mixed salt remains in a liquid state at the investigated temperature of 700 °C according to the hypothetical phase diagram of the NaCl/ $\text{Na}_2\text{SO}_4$  system

**Fig. 9** EDS mapping for IOZ of **a** 0Nb and **b** 0.8Nb weld metals after being exposed to molten  $\text{Na}_2\text{SO}_4\text{-NaCl}$  salt mixture at  $700^\circ\text{C}$  for 100 h

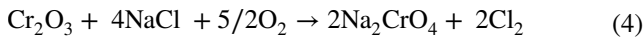


**Fig. 10** schematic diagram for the hot corrosion mechanism of the weld metal with different Nb contents in 75 wt% $\text{Na}_2\text{SO}_4\text{-}25$  wt% $\text{NaCl}$  molten salt at  $700^\circ\text{C}$

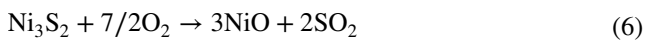
[32]. The following reactions could occur in the interface of the molten salts and oxide film [33].







$\text{Na}_2\text{FeO}_4$  and  $\text{Na}_2\text{CrO}_4$  are volatile substances and will diffuse into the air. Amounts of pores appear in the oxide layer (Fig. 6). Then O,  $\text{Cl}_2$  and  $\text{SO}_2$  diffuse through the damaged bilayer oxide scale into the matrix of weld metals. According to the Ellingham diagram [34], Si-oxide and Cr-oxide have a low oxygen partial pressure. Si and Cr could react with oxygen to form oxides under surface oxide film. Considering the unique microstructures of investigated weld metal, the interdendritic zone, which could be acted as a subgrain boundary, may provide a diffusion pass for ions at high temperatures [35]. O could diffuse into the matrix along the interdendritic zones or grain boundaries. Hence, a large IOZ appears under the oxide film. With the diffusion of element S, the concentration gradient of S is formed in the IOZ of the weld metal in the molten salt environment. Once the oxygen partial pressure in a certain area of the weld metal matrix is lower than a critical value, the sulfide will be generated there. The following reactions could occur in the matrix [36].



Equation (5) explains the distribution coincidence of elements S and Ni in Fig. 9b. It is worth noting that sulfide is just found in the interface of IOZ and matrix (Fig. 9), which could be attributed to the fact that sulfide can be oxidized to oxide according to Eq. (6) when oxygen partial pressure is again up to a critical value. In a word, oxidation and sulfidation occur in the matrix due to the inward diffusion of O and S when Fe–Cr–Ni-based weld metal was exposed to 700 °C in  $\text{Na}_2\text{SO}_4$ –NaCl molten salts. Non-equilibrium weld metal suffers severe hot corrosion.

With Nb addition to the weld metal, Nb could combine with O to form  $\text{Nb}_2\text{O}_5$  under the  $\text{Cr}_2\text{O}_3$  layer due to its lower oxygen partial pressure [37]. The Pilling-Bedworth ratio (PBR) is generally used to evaluate the growth stress of oxides [38]. The PBR for  $\text{Nb}_2\text{O}_5$  is about 2.67, indicating that a large compressive stress would be induced in the surface oxide film [21]. As shown in Figs. 6b and 10, cracks are formed in the oxide layer of the Nb-bearing weld metal.  $\text{O}_2$  in the air will diffuse into the matrix rapidly through the cracks and amounts of Cr and Fe will be consumed to form (Cr, Fe)-oxide. A thick bilayer oxide scale then formed on the surface of the Nb-bearing weld metal (Fig. 6). Further, Nb promotes the Nb(C, N) primary phase to precipitate along the interdendritic zone according to the microstructure observation (Fig. 3). Nb(C, N) particles distributing in chains may provide a diffusion pass for O and S. Oxidation and sulfidation occur preferentially near the Nb(C, N) particles and promote the formation of large oxides or sulfides,

as shown in Fig. 7. Of course, Nb(C, N) close to surface is easy to be oxidized to the Nb oxide. Hence, no Nb(C, N) particles could be observed close to the surface oxide layer.

## 4 Conclusions

In the present work, the effect of Nb on the microstructure and hot corrosion behavior of the Fe–Cr–Ni-based weld metal in the 75 wt% $\text{Na}_2\text{SO}_4$ –25 wt%NaCl molten salt at 700 °C was investigated. The following conclusions based on the results and discussions could be drawn:

1. Nb prevents the Cr-carbide from precipitating at grain boundaries and promotes the formation of Nb(C, N) distributing along the interdendritic zone in the Fe–Cr–Ni-based weld metal.
2. A bilayer oxide scales composed of an inner  $\text{Cr}_2\text{O}_3$  layer and an outer  $\text{Fe}_2\text{O}_3$  layer formed on the surface of the Fe–Cr–Ni-based weld metal after being exposed to 700 °C in the  $\text{Na}_2\text{SO}_4$ –NaCl molten salt for 100 h. With Nb addition, the thickness of the bilayer oxide film becomes larger. Nb has an adverse effect on the hot corrosion resistance of the investigated weld metal in molten salt.
3. Oxidation and sulfidation occur in the matrix of the austenitic weld metal due to the inward diffusion of O and S. Element Nb seemingly promote the occurrence of the sulfidation reaction, which could be attributed to the short-circuit diffusion of S through the interface of Nb(C, N) and matrix.
4. An apparent Cr-dealloyed layer appears in the IOZ of the Fe–Cr–Ni-based weld metal. Alloying with 0.8 wt% of Nb further accelerated the dealloying and resulted in a profound attack.

**Acknowledgements** This work is supported by the Natural Science Foundation of Jiangsu Province (Grant No. BK20201036), the Special Talent Introduction for “Double Innovation Plan” in 2020, the Opening Project of Jiangsu Key Laboratory of Advanced Structural Materials and Application Technology (ASMA202007) and the Introduction of Talent Research Fund at Nanjing Institute of Technology (YKJ201954).

## Declarations

**Conflict of interest** The authors declare that they have no conflict of interest.

## References

1. S.A. David, J.A. Siefert, Z. Feng, Welding and weldability of candidate ferritic alloys for future advanced ultrasupercritical fossil power plants. *Sci. Technol. Weld. Join.* **18**(8), 631–651 (2013)

2. D. Wu, D. Li, S.P. Lu, Microstructural evolution and mechanical property of a Ni-Fe-based weld metal during long-term exposure at 650 °C and 700 °C. *Mater. Sci. Eng. A* **716**, 240–251 (2018)
3. H. Ma, Y. Wang, Z. Liang, Q. Zhao, Z. Ke, Investigation on high temperature corrosion characteristic of super304H, TP347H, and HR3C steel in an ultra-supercritical coal-fired boiler. *Fuel Cells* **21**(1), 24–30 (2021)
4. D. Wu, D. Li, S.P. Lu, Effect of Cr content on the microstructural stability and impact-toughness evolution of a Ni-Fe-based weld metal. *J. Alloy. Compd.* **749**, 465–472 (2018)
5. S. Ueda, K. Kadoi, S. Tokita, H. Inoue, Relationship between alloy element and weld solidification cracking susceptibility of austenitic stainless steel. *ISIJ Int.* **59**(7), 1323–1329 (2019)
6. J.C.F. Jorge, J.L.D. Monteiro, A.J. de Carvalho Gomes, I. de Souza Bott, L.F.G. de Souza, M.C. Mendes, L.S. Araújo, Influence of welding procedure and PWHT on HSLA steel weld metals. *J. Mater. Res. Technol.* **8**(1), 561–571 (2019)
7. X.X. Zhang, L.H. Wu, H. Andrä, W.M. Gan, M. Hofmann, D. Wang, D.R. Ni, B.L. Xiao, Z.Y. Ma, Effects of welding speed on the multi-scale residual stresses in friction stir welded metal matrix composites. *J. Mater. Sci. Technol.* **35**(5), 824–832 (2019)
8. Y.L. Sun, G. Obasi, C.J. Hamelin, A.N. Vasileiou, T.F. Flint, J. Balakrishnan, M.C. Smith, J.A. Francis, Effects of dilution on alloy content and microstructure in multi-pass steel welds. *J. Mater. Process. Technol.* **265**, 71–86 (2019)
9. H. Liu, K. Guo, J. Sun, H. Shi, Effect of Nb addition on the microstructure and mechanical properties of Inconel 718 fabricated by laser directed energy deposition. *Mater. Charact.* **183**, 111601 (2022)
10. T. Patterson, J.C. Lippold, Effect of niobium on the microstructure and properties of submerged arc welds in HSLA steel. *Weld. World* **64**(6), 1089–1105 (2020)
11. J. Zhang, Z. ur Rahman, X. Wang, Z. Wang, P. Li, Y. Wang, D. Bate, K. Zhao, Houzhang Tan, Hot corrosion behaviors of TP347H and HR3C stainless steel with KCl deposit in oxy-biomass combustion. *J. Environ. Manag.* **263**, 110411 (2020)
12. T. Ghaznavi, S.Y. Persaud, R.C. Newman, The effect of temperature on dealloying mechanisms in molten salt corrosion. *J. Electrochem. Soc.* **169**(11), 111506 (2022)
13. H. Sun, J. Liu, Hot corrosion of Fe and Ni-based alloys in Waste-to-energy environment at 850 °C. *Eng. Fail. Anal.* **133**, 105964 (2022)
14. M. Sarvghad, T.A. Steinberg, G. Will, Corrosion of steel alloys in eutectic NaCl+ Na<sub>2</sub>CO<sub>3</sub> at 700 °C and Li<sub>2</sub>CO<sub>3</sub>+ K<sub>2</sub>CO<sub>3</sub>+ Na<sub>2</sub>CO<sub>3</sub> at 450 °C for thermal energy storage. *Sol. Energy Mater. Sol. Cells* **170**, 48–59 (2017)
15. T. Ghaznavi, M.A. Bryk, S.Y. Persaud, R.C. Newman, Alloying effects in high temperature molten salt corrosion. *Corros. Sci.* **197**, 110003 (2022)
16. C.-C. Tsauro, J.C. Rock, C.-J. Wang, Y.-H. Su, The hot corrosion of 310 stainless steel with pre-coated NaCl/Na<sub>2</sub>SO<sub>4</sub> mixtures at 750 °C. *Mater. Chem. Phys.* **89**(2–3), 445–453 (2005)
17. J.H. Wang, D.G. Li, T.M. Shao, Electrochemical study on the hot corrosion behavior of Ni16Cr13Co4Mo alloy in molten NaCl-KCl and NaCl-KCl-Na<sub>2</sub>SO<sub>4</sub>. *Corros. Sci.* **200**, 110247 (2022)
18. Y. Zhou, H. Wang, C. Mo, L. Zhang, Effect of minor Nb on isothermal-oxidation and hot corrosion behavior of two nickel-based superalloys under Na<sub>2</sub>SO<sub>4</sub>/Na<sub>2</sub>SO<sub>4</sub>-NaCl. *Corrosion* **77**(9), 949–960 (2021)
19. Y.-X. Xu, J.-T. Lu, X.-W. Yang, J.-B. Yan, W.-Y. Li, Effect and role of alloyed Nb on the air oxidation behaviour of Ni-Cr-Fe alloys at 1000 °C. *Corros. Sci.* **127**, 10–20 (2017)
20. J. Dai, H. Zhang, C. Sun, S. Li, C. Chen, Y. Yang, The effect of Nb and Si on the hot corrosion behaviors of TiAl coatings on a Ti-6Al-4V alloy. *Corros. Sci.* **168**, 108578 (2020)
21. G. Jia, W. Xu, M. Ouyang, H. Wang, L. Wang, X. Xiao, Oxidation behavior of Ni-25Cr-10Fe-3Si- $\chi$ Nb alloys at 1000 °C in ambient air: role of Laves phase. *Corros. Sci.* **187**, 109475 (2021)
22. Y.X. Xu, J.T. Lu, W.Y. Li, X.W. Yang, Oxidation behaviour of Nb-rich Ni-Cr-Fe alloys: role and effect of carbides precipitates. *Corros. Sci.* **140**, 252–259 (2018)
23. R.A. Wheeling, J.C. Lippold, Characterization of weld metal microstructure in a Ni-30Cr alloy with additions of niobium and molybdenum. *Mater. Charact.* **115**, 97–103 (2016)
24. D. Wu, D.Z. Li, S. Lu, Microstructures and intermediate temperature brittleness of newly developed Ni-Fe based weld metal for ultra-supercritical power plants. *Mater. Sci. Eng. A* **684**, 146–157 (2017)
25. X. Zhang, D.Z. Li, Y.Y. Li, S. Lu, The influence of niobium on the plastic deformation behaviors of 310s austenitic stainless steel weld metals at different temperatures. *Mater. Sci. Eng. A* **743**, 648–655 (2019)
26. C. Han, Q. Liu, Z. Cai, X. Huo, M. Fan, K. Li, J. Pan, Effect of solidification segregation on microstructure and mechanical properties of a Ni-Cr-Mo-V steel weld metal. *Metall. Mater. Trans. A.* **53**(4), 1394–1406 (2022)
27. W. Zhang, Y. Yang, Y. Tan, S. Xiang, W. Shi, M. Ma, Hot corrosion behavior and mechanism of cryo-rolled MP159 superalloy with long rod-like  $\gamma'$  phase. *Corros. Sci.* **209**, 110706 (2022)
28. X.H. Li, S.M. Wang, B.B. Xue, Technology of electrochemical micromachining based on surface modification by fiber laser on stainless steel. *Mater. Sci. Forum* **909**, 67–72 (2017)
29. Y. Zhang, H. Wu, X. Yu, D. Tang, Role of Cr in the high-temperature oxidation behavior of CrxMnFeNi high-entropy alloys at 800 °C in air. *Corros. Sci.* **200**, 110211 (2022)
30. C. Stephan-Scherb, W. Schulz, M. Schneider, S. Karafiludis, G. Laplanche, High-temperature oxidation in dry and humid atmospheres of the equiatomic CrMnFeCoNi and CrCoNi high- and medium-entropy alloys. *Oxid. Met.* **95**, 105–133 (2021)
31. A. Neville, F. Reza, S. Chiovelli, T. Revega, Characterization and corrosion behavior of high-chromium white cast irons. *Metall. Mater. Trans. A* **37**, 2339–2347 (2006)
32. W. Kai, C.H. Lee, T.W. Lee, C.-H. Wu, Sulfidation behavior of Inconel 738 superalloy at 500–900 °C. *Oxid. Met.* **56**, 51–71 (2001)
33. S. Hu, H. Finklea, X. Liu, A review on molten sulfate salts induced hot corrosion. *J. Mater. Sci. Technol.* **90**, 243–254 (2021)
34. M. Hasegawa, Ellingham diagram, in *Treatise on Process Metallurgy*, ed. by S. Seetharaman (Elsevier, Amsterdam, 2014), pp.507–516
35. S. Pour-Ali, A.R. Kiani-Rashid, A. Babakhani, M. Norouzi, S. Virtanen, New insights into the effects of surface nanocrystallization on the oxidation of 321 austenitic stainless steel in a humid oxygen environment at 1000 °C. *Corros. Sci.* **147**, 231–245 (2019)
36. X. Lu, S. Tian, Tao Chen, C. Guo, G. Li, Internal oxidation and internal sulfuration of Ni-base alloy with high Cr content during hot corrosion in molten sulfate. *Rare Met. Mater. Eng.* **43**(1), 79–84 (2014)
37. T.-H. Kim, M.Z. Khan, R.-H. Song, S.-B. Lee, T.-H. Lim, J.-E. Hong, Development of oxide dispersed ferritic steel as a solid oxide fuel cell interconnect. *ECS Trans.* **91**(1), 2307 (2019)
38. C. Xu, W. Gao, Pilling-Bedworth ratio for oxidation of alloys. *Mater. Res. Innov.* **3**(4), 231–235 (2000)

**Publisher's Note** Springer Nature remains neutral with regard to jurisdictional claims in published maps and institutional affiliations.

Springer Nature or its licensor (e.g. a society or other partner) holds exclusive rights to this article under a publishing agreement with the author(s) or other rightsholder(s); author self-archiving of the accepted manuscript version of this article is solely governed by the terms of such publishing agreement and applicable law.